ACS Catalysis

Perspective

pubs.acs.org/acscatalysis

Catalyzing the Hydrogen Evolution Reaction (HER) with Molybdenum Sulfide Nanomaterials

Jesse D. Benck,[†] Thomas R. Hellstern,[†] Jakob Kibsgaard, Pongkarn Chakthranont, and Thomas F. Jaramillo*

Department of Chemical Engineering, Stanford University, 443 Via Ortega, Stanford, California 94305, United States

ABSTRACT: We discuss recent developments in nanostructured molybdenum sulfide catalysts for the electrochemical hydrogen evolution reaction. To develop a framework for performing consistent and meaningful comparisons between catalysts, we review standard experimental methodologies for measuring catalyst performance and define two metrics used in this perspective for comparing catalyst activity: the turnover frequency, an intrinsic activity metric, and the total electrode activity, a device-oriented activity metric. We discuss general strategies for synthesizing catalysts with improved activity, namely, increasing the number of electrically accessible active sites or increasing the turnover frequency of each site. Then we consider a number of state-of-the-art molybdenum sulfide catalysts, including crystalline MoS_2, amorphous MoS_x, and molecular cluster materials, to highlight these strategies in practice. Comparing these catalysts reveals that most of the molybdenum sulfide catalysts have similar active site turnover frequencies, so the total electrode activity is primarily determined by the number of accessible active sites per geometric electrode area. Emerging strategies to overcome current catalyst limitations and potential applications for molybdenum sulfide catalysts including photoelectrochemical water splitting devices and electrolyzers are also considered.

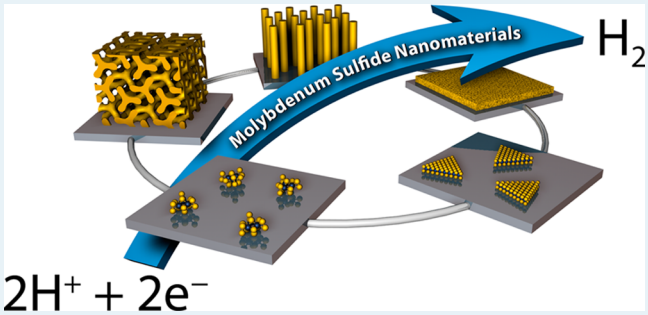

KEYWORDS: *molybdenum sulfide, hydrogen evolution, electrocatalysis, water splitting, nanomaterials*

1. INTRODUCTION

Supplying the world's growing population with clean, affordable energy is a critical challenge.[1] Global energy demand is projected to rise from 17 TW in 2010 to 27 TW by 2040.[2] Fossil fuels continue to dominate the global energy landscape, but increasing concerns over the effect of anthropogenic carbon dioxide on the earth's climate make sustainable energy technologies, such as wind and solar, attractive options.[3−6] However, the challenges of energy storage and integration into the current power grid have hindered the implementation of these intermittent renewable energy sources.[4,7,8] Electrochemical and photoelectrochemical water splitting are promising ways to store sustainable, intermittent energy resources (e.g., wind and solar) in the form of hydrogen, an energy vector with high energy density and potentially without carbon emissions.[9−11] However, substantial technological advancements are necessary to make widespread implementation of water splitting economically viable. One critical requirement is the development of highly active, stable electrocatalysts composed of earth-abundant materials.[9]

In this perspective, we discuss molybdenum sulfide electrocatalysts for the hydrogen evolution reaction (HER). Other dichalcogenides such as tungsten sulfide (WS_2) have shown promise as HER catalysts,[12−15] but they will not be discussed here. Due to their high activity, excellent stability, and precious metal-free composition, molybdenum sulfide materials represent a promising class of materials for making electrochemical hydrogen production feasible. There have been many important developments in MoS_2 HER catalysis in recent years, many of which have been reviewed elsewhere.[15−18] In this perspective, we aim to provide a framework for evaluating and comparing strategies for improving the activity of molybdenum sulfide HER catalysts. We begin by discussing best practices for measuring the activity of HER catalysts, then highlight a number of specific studies to illustrate important approaches for developing MoS_2 catalysts with improved activity. We consider crystalline, amorphous, and molecular cluster molybdenum sulfide materials. To evaluate the efficacy of the various strategies for enhancing activity, we compare a number of the most successful catalysts using two metrics: the turnover frequency, an intrinsic activity metric, and the overpotential required to reach 10 $mA/cm^2_{electrode}$, a device-oriented total electrode activity metric. Finally, we discuss emerging directions in MoS_2 catalysis.

2. BACKGROUND

2.1. Water Splitting. Electrochemical water splitting can be performed in a variety of devices, which can be broadly

Received: June 29, 2014
Revised: August 25, 2014
Published: October 8, 2014

   dx.doi.org/10.1021/cs500923c | ACS Catal. 2014, 4, 3957−3971

classified into two main categories: water electrolysis and water photolysis. Water electrolyzers, which include polymer electrolyte membrane (PEM), alkaline, and solid oxide electrolyzer configurations, require energy input from an external source of electricity to drive the water splitting process.[19−21] Photoelectrochemical (PEC) and photocatalytic water splitting devices rely on semiconductor materials to absorb sunlight and generate exited charge carriers, and can therefore split water without an external electricity input.[9,22] Regardless of the device configuration, the overall water splitting reaction remains the same:

$$H_2O \rightarrow H_2 + \frac{1}{2}O_2$$

This reaction requires an energy input of ΔG = 237.1 kJ/mol at standard conditions, which corresponds to a thermodynamic voltage requirement of 1.23 V.[9,23,24] In a water splitting cell, the hydrogen evolution reaction (HER) takes place at the cathode and the oxygen evolution reaction (OER) takes place at the anode. These reactions are shown below (Table 1) as they occur in acidic electrolyte:

Table 1

hydrogen evolution reaction (HER)	$2H^+ + 2e^- \rightarrow H_2$
oxygen evolution reaction (OER)	$H_2O \rightarrow \frac{1}{2}O_2 + 2H^+ + 2e^-$

To split water efficiently, catalysts are required for both the HER and the OER. Developments in OER catalysis have been discussed elsewhere;[9,25] in this perspective we focus on the HER.

2.2. Hydrogen Evolution Reaction. The hydrogen evolution reaction is thought to involve three possible reaction steps (Table 2):[26]

Table 2

1	Volmer step	$H^+ + e^- \rightarrow H_{ad}$
2	Heyrovsky step	$H^+ + H_{ad} \rightarrow H_2$
3	Tafel step	$2H_{ad} \rightarrow H_2$

The HER may occur via the Volmer−Heyrowsky mechanism or the Volmer−Tafel mechanism. In both cases, the reaction proceeds through hydrogen atoms adsorbed at the electrode surface, H_{ad}, and thus the rate of the overall reaction is influenced by the free energy of hydrogen adsorption, ΔG_H, as originally described by Parsons.[27] If the hydrogen to surface bond is too weak, the adsorption step will limit the overall reaction rate. If the hydrogen to surface bond is too strong, the reaction−desorption step will limit the overall reaction rate. Optimal HER catalysts have hydrogen adsorption energies close to $\Delta G_H = 0$, binding hydrogen neither too weakly nor too strongly.[16,17,28−30] This principle gives rise to the "volcano" relationship in Figure 1, which shows the HER exchange current (a measure of catalytic activity) as a function of ΔG_H. To maximize the rate of the HER, a catalyst with appropriate surface properties must be employed. Several classes of materials have been investigated as active HER catalysts, including precious metals such as platinum, nickel alloys, metal oxides, metal phosphides, and metal sulfides; many of these efforts have been reviewed previously.[9,31]

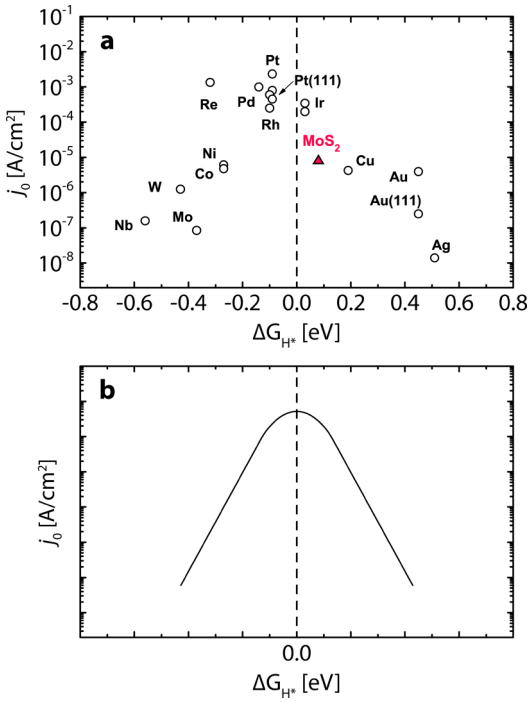

Figure 1. Exchange current density as a function of hydrogen adsorption free energy for various HER catalyst materials. (a) The experimental "volcano plot" for the HER is shown and Pt, with slightly negative hydrogen absorption energy, has the highest HER activity.[36] (b) The theoretical HER volcano, adapted from Parsons, predicts catalysts with hydrogen binding energy equal to zero will have the highest activity.[27] Further details concerning metrics for catalyst activity are given in section 3.1. Reproduced with permission.[36]

2.3. Molybdenum Disulfide. MoS_2 has many interesting properties that allow it to be exploited as a lubricant,[32] 2D transistor,[33] and hydrodesulfurization catalyst,[34] but this review will focus on MoS_2 as a HER catalyst. Interestingly, early work on the electrochemistry of bulk MoS_2 crystals by Tributsch[35] and others suggested that this material is not an active HER catalyst, but interest has been revived as studies have shown that nanostructuring MoS_2 materials can significantly improve HER activity.[36,37]

Bulk MoS_2 is a hexagonally packed layered structure, similar to graphite, with a 6.5 Å van der Waals gap separating each sheet as shown in Figure 2.[38−40] As a result of this crystal structure, MoS_2 possesses a variety of distinct surface sites and electron and hole mobilities approximately 2200 times faster along a basal plane than perpendicularly between sheets.[41] The surface of bulk MoS_2 primarily consists of the thermodynamically favored basal plane sites, which are catalytically inert.[35,42,43] In contrast, the edges of MoS_2 layers have high activity for the HER.[37]

In their seminal work on MoS_2 for the HER, Hinnemann and co-workers calculated, using density functional theory (DFT), that the Mo($\bar{1}$010) edge of MoS_2 possesses a hydrogen binding energy of approximately 0.08 eV at 50% H coverage, very close to the optimum value of 0 eV.[37] This binding energy is similar to that observed on active precious metal catalysts, including Pt.[37] This work was inspired by enzymes such as hydrogenases and nitrogenases, both of which are effective hydrogen producing catalysts.[44−46] Both of these classes of enzymes are highly active, have hydrogen binding energies close to zero, and possess motifs containing Mo, Ni, and Fe with under-

dx.doi.org/10.1021/cs500923c | ACS Catal. 2014, 4, 3957−3971

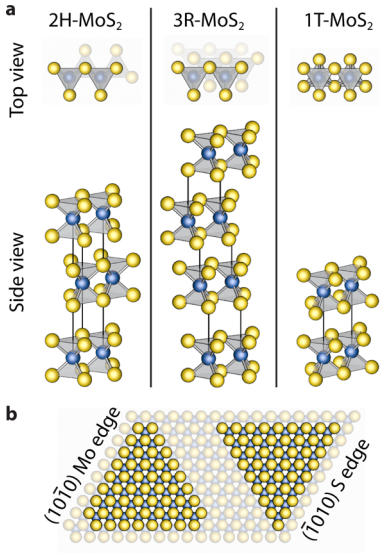

Figure 2. (a) Structure of the 2H, 3R, and 1T polytypes of MoS_2. (b) Top view of the Mo edge and S edge of a bulk MoS_2 crystal.

coordinated sulfur at their active sites. Guided by the MoS_2 edge site prediction, experimentalists synthesized MoS_2 on a high surface area carbon black support to expose a large number of edge sites.[37] Their membrane electrode assembly setup, which reduced protons to make hydrogen at the cathode and oxidized hydrogen at the anode achieved 10 $mA/cm^2_{electrode}$ at about 175 mV overpotential, the most active, acid stable, nonprecious metal catalyst for the HER at the time.

In 2007, it was experimentally confirmed that the MoS_2 edges are active catalysts for the HER by depositing single monolayer MoS_2 nanoparticles on Au(111) synthesized by physical vapor deposition of Mo in an H_2S environment.[36] After quantifying the nanoparticle area and edge length using scanning tunneling microscopy (STM), they measured the HER activity and confirmed that the reaction rate scaled with perimeter length rather than area. The per-site activity (turnover frequency) of MoS_2 edges was very high, yet still 50−100 times lower than that of Pt.[47] The insights gained by means of theory and fundamental experimental studies consequently sparked significant efforts aimed at developing MoS_2 catalysts with improved activity approaching that observed for platinum surfaces.

3. PARAMETERS FOR CATALYST ACTIVITY COMPARISONS

There are many performance characteristics that may be important in evaluating an electrocatalyst material's efficacy for a particular application, including its activity, stability, selectivity, cost, and optical or mechanical properties. Catalytic activity is almost always critical, however there is no universal method for assessing the activity of HER catalysts.[48,49] A variety of methodologies are described in the literature, and the differences among these strategies can make it challenging to compare different catalysts in a consistent manner.[12,16,17,36,37,50−76] Furthermore, all activity comparison approaches have advantages and disadvantages, so it is important to choose an appropriate strategy based on the relevant performance metrics for a given system. In this section, we first briefly review standard methodologies employed for measuring HER electrocatalyst activity. Then, we focus on two particularly important activity metrics to provide a fair and useful framework for comparing molybdenum sulfide HER catalysts.

The two primary categories of activity measurements of interest in this work are "total electrode" activity (i.e., geometric electrode area-normalized measurements) and "intrinsic" activity (i.e., per-site turnover frequency, TOF). Total electrode activity measurements are useful for practical device performance comparisons, but they are not ideal for fundamental studies of novel catalyst materials because they do not reveal the physical or chemical origins of an electrode's activity. Intrinsic activity measurements provide the activity of the catalyst on a per-site basis, and therefore contribute to the molecular-level structure-property-function relationships necessary to guide catalyst development. As shown in Figure 3, these

$$j(\eta) = \frac{i(\eta)}{A} = \left[\sum_{x=1}^{S} TOF_x(\eta)\right] \cdot \frac{nF}{AN_A} = S \cdot \overline{TOF}(\eta) \cdot \frac{nF}{AN_A}$$

j	catalytic current density ($A/cm^2_{electrode}$)
i	catalytic current (A)
η	overpotential (V)
A	superficial electrode area ($cm^2_{electrode}$)
S	number of surface sites
n	number of electrons tranferred per molecule, 2 for HER
F	Faraday constant, 96458 (C/mol electrons)
N_A	Avogadro's number, $6.022 \cdot 10^{23}$ (mol^{-1})
TOF_x	turnover frequency of site x (s^{-1})
$\overline{TOF}$	average turnover frequency of all sites (s^{-1})

Figure 3. Equation relating HER current and turnover frequency of each catalytic site. In practice, it is easiest to measure the current and number of surface sites, then derive the average turnover frequency per site.[54]

two classes of activity measurements are fundamentally related, as the total electrode activity of any HER catalyst is determined by the product of two factors: the number of active sites and the intrinsic activity (turnover frequency) of each site. Intrinsic activity measurements deconvolute these two factors and thus provide more information, but such measurements can be challenging to perform accurately.

3.1. Total Electrode Activity Measurements. Total electrode activity measurements are useful for comparing complete electrodes and are typically the first step in characterizing HER catalyst materials. These measurements are usually performed by supporting the catalyst on an inert, conducting substrate and performing cyclic voltammetry or linear sweep voltammetry to measure the catalytic current as a function of potential. For water-splitting reactions, it is most appropriate to calibrate the potential scale to the reversible hydrogen electrode (RHE). The current is often normalized to the superficial geometric electrode area to facilitate comparison between materials tested under different experimental conditions.

Although the full cyclic voltamograms (CV) or linear sweep voltamograms (LSV) contain the most complete information about catalyst activity, it is often helpful to report measurements at certain specific potentials to facilitate comparison among catalyst materials. Some special potentials are noted in Figure 4. One potential of interest is the "onset potential," or the potential at which catalytic current is first observed. Without a strict definition, the ambiguity of the onset potential makes it a poor criterion for comparing different catalysts;

dx.doi.org/10.1021/cs500923c | ACS Catal. 2014, 4, 3957−3971

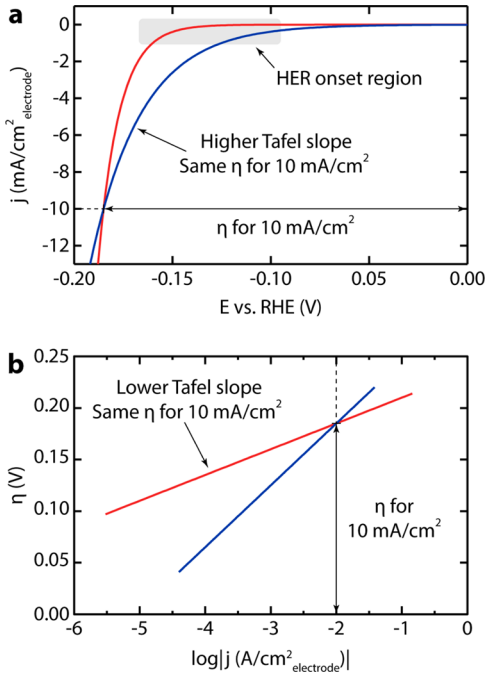

Figure 4. HER activity of two theoretical catalysts. (a) Representative linear sweep voltamograms (LSV) plotting current density as a function of potential. (b) Tafel plot. These catalysts require the same overpotential for −10 mA/cm$^2_{electrode}$, so they appear the same based on the total electrode activity metric used in this perspective. However, these catalysts likely have different HER mechanisms based on their different Tafel slopes, and both could be better or worse than the other depending on the application. The catalyst represented in blue would perform better for low current devices (<10 mA/cm$^2_{electrode}$), whereas the catalyst represented in red would be superior for high current density devices (>10 mA/cm$^2_{electrode}$).

different observers may assign different onset potentials to the same data and non-Faradaic capacitive current may constitute a significant fraction of the total current in the onset region. Thus, the onset potential should always be defined on the basis of a specific current density. Depending on the surface area of the catalyst and scan rate of the LSV, a suitable current value for the onset could range from 0.05−5 mA/cm^2 (e.g., 0.1 mA/cm^2). A more relevant metric by which to compare catalysts is the potential required to reach an operating current density of interest. In solar water splitting, the potential for 10 mA/cm$^2_{electrode}$ is a common figure of merit because this is the current density expected in a 12.3% efficient solar to hydrogen device, which is on the order of the efficiency that would be required for cost competitive photoelectrochemical water splitting.[9,50,54,77−80] In this perspective, we use the 10 mA/cm^2 metric to compare the total electrode activities of the MoS_2 HER catalysts. The potential to reach a different current density may be more relevant for catalysts intended for application in water electrolyzers, which typically operate at current densities on the order of 1−2 A/cm^2.[19]

The exchange current density and Tafel slope are also frequently reported total electrode activity metrics.[59,63,81,82] The specific value of the electrode area-normalized exchange current density in the absence of other critical information is not an ideal metric for ranking catalyst activity since it is neither a relevant practical performance parameter nor a fundamental material property, as it depends on both the per-site turnover frequency and the total number of sites. However, recognizing that the site-specific exchange current density can vary by 10 orders of magnitude between a good catalyst and a bad catalyst, and that the total number of active sites on an electrode typically only varies by 2−3 orders of magnitude between a flat catalyst film and a nanostructured film, a high total electrode exchange current density is a necessary, but insufficient, condition for highly active electrodes. In combination with the Tafel slope, the electrode area-normalized exchange current density can be an informative parameter. When applied in the Tafel equation, these two metrics together can be used to calculate the overpotential required to achieve any current density. However, changes in the Tafel slope as a function of potential due to transport limitations, changes in catalyst surface structure, or other effects may introduce errors in this calculation, and the same information can usually be obtained more directly from the measured current−voltage curves. From a practical perspective, the Tafel slope determines the additional voltage required to increase the catalytic current by an order of magnitude, with units commonly reported in mV/decade. Ultimately, all electrodes are judged by the overpotential required to reach an operating current density, which is determined by both its Tafel slope and onset potential. Therefore, low Tafel slopes are desirable, especially for high current applications such as water electrolyzers. As demonstrated in Figure 4, catalysts with different Tafel slopes could still end up requiring the same amount of overpotential to reach 10 mA/cm$^2_{electrode}$. Under certain conditions using model HER catalyst systems, the Tafel slope may also provide evidence of a particular reaction mechanism. However, in most cases the Tafel slope alone cannot be used to unambiguously identify the mechanism in the absence of additional experiments.[50,54]

In summary, for total electrode activity measurements the most relevant metric by which to compare catalysts is the potential to reach a current density of interest, for example, 10 mA/cm$^2_{electrode}$, for HER catalysts intended for solar fuels applications. As there is no normalization to the amount of catalyst loaded per geometric area, it follows that electrodes with very high catalyst loadings typically have the highest total electrode activity.

3.2. Intrinsic Activity Measurements. The ideal means to understand catalyst performance is by measuring the activity of each catalytic site and relating it to the site's physical and chemical properties. For nonprecious metal catalysts, total electrode activity is the most important metric for device-oriented catalyst development. The intrinsic activity of each catalytic site is more important to develop a fundamental understanding of the origins of a material's catalytic activity, which is necessary to design highly active electrodes. Unfortunately, limitations of current experimental techniques make this task challenging. Most practical catalysts include many different types of surface sites, each with their own inherent activity, and there are few experimental techniques to probe individual sites. Different methods are required for different materials, measurements are often complicated by non-Faradaic current, catalyst instability, and/or transport limitations. The most common strategy for determining intrinsic per-site activity is to first measure the total electrode activity and then, through a separate measurement, to determine the total number of active sites and use these results to infer the average TOF. Although this method is less powerful than the ideal measurement, this strategy still enables the

dx.doi.org/10.1021/cs500923c | ACS Catal. 2014, 4, 3957−3971

development of relationships between material properties and catalytic activity to drive further catalyst design efforts.

3.2.1. Measuring the Number of Active Sites. All intrinsic activity measurements include some effort to determine the number of active sites. In most cases, such a measurement is approximate rather than precise. Sometimes related quantities such as mass loading, total surface area, or electrochemically active surface area (ECSA) may also be employed in place of the number of active sites. Some of the relevant measures of surface area are illustrated in Figure 5.

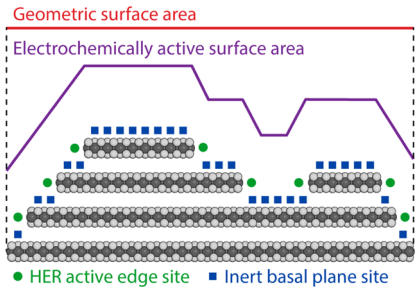

Figure 5. Two-dimensional representation of MoS_2 catalyst electrochemically active surface area and projected geometric surface area. For crystalline 2H-MoS_2, only edge sites, indicated by green dots, are active for HER. Basal plane sites, indicated by blue squares, are not active for HER. Rougher surfaces should have more available edge sites and thus higher catalytic activity per projected geometric surface area. It should also be noted that a catalyst geometry with basal planes oriented perpendicular to the surface would result in a more active catalyst, but the less active geometry is displayed here for visualization purposes.

Normalizing the total electrode activity by the catalyst mass is important as a practical performance metric for precious metal-based catalysts where the cost of the catalyst material is a primary concern.[83] To perform these measurements, the electrode-supported catalyst material is often dissolved off of the electrode surface, and its mass is measured using an established method of quantitative chemical analysis, for instance, by means of inductively coupled plasma optical emission spectroscopy (ICP-OES) or a related technique. Mass normalization is less common for nonprecious materials like molybdenum sulfides because the catalyst mass is not as critical to the cost of the device. Catalyst mass measurements, however, may still be used as a means to estimate the total number of active sites, which is the key parameter for understanding catalyst property-performance relationships. Although helpful, this technique is typically not the optimal strategy for intrinsic activity measurements because the number of active sites might not scale linearly with mass loading due to variations in catalyst morphology.

Measuring the total catalyst surface area or its electrochemically active surface area (as opposed to the superficial geometric electrode area) is one of the most common approaches for estimating the number of catalytic sites in nonprecious materials.[50,58,70] This is an appropriate strategy because the number of active sites often scales with the catalyst surface area. Methods for measuring active surface area include both gaseous adsorption and electrochemical techniques. Gaseous adsorption techniques such as BET, which rely on the adsorption of probe molecules (e.g., N_2) at the catalyst surface, are excellent for heterogeneous catalyst materials and may be useful for some electrocatalysts, but these techniques can potentially overestimate the active surface area by adsorbing to some material that is not in electrical contact to the substrate and therefore cannot catalyze the reaction.[84,85] Overestimating surface area in this case would lead to a conservative estimate of the TOF. Electrochemical measurements are often preferred because they directly probe the electrochemically active surface area (ECSA).[84] One popular technique involves measuring the non-Faradaic current associated with electrochemical double layer charging at the catalyst surface.[50,58,70,84] This value can be compared to the material's specific capacitance determined using a flat reference material to determine the catalyst's ECSA. Electrochemical probe molecule adsorption is another common technique. The most prevalent example of this strategy is hydrogen underpotential deposition, a standard method for measuring the surface area of platinum electrocatalysts.[86] Other common probe molecule techniques include underpotential deposition of lead or copper and carbon monoxide stripping, which involves adsorption and electrooxidation.[87−90] Unfortunately, these methods are not universally applicable to all materials. Although the conditions used for these electrochemical surface area measurement techniques generally approximate HER operating conditions better than those used for gaseous adsorption techniques, these electrochemical measurements may still be imperfect because factors such as the catalyst surface structure or active site accessibility could change between the surface area measurement conditions and the operating conditions.

In some cases, the electrocatalyst contains structurally or chemically heterogeneous sites with substantially different TOFs. Under these circumstances, techniques that enable a direct determination of the number of active sites are preferred to surface area measurements because the number of active sites may not scale directly with the overall surface area or ECSA. This is the case with MoS_2 HER catalysts, which generally consist of edge sites that are catalytically active for the HER and basal plane sites which are inert. In some studies, the number of active MoS_2 edge sites has been estimated using scanning tunneling microscopy or transmission electron microscopy imaging.[36,54] Other studies have employed electrochemical oxidation of the MoS_2, yielding distinct electrochemical features corresponding to the edge sites and the basal plane sites.[52] The number of edge sites was determined by integrating the appropriate oxidative feature. Other works have used probe molecules such as copper ions that adsorb selectively to the active sites,[14] though the reliability of these techniques has not been well-established for molybdenum sulfide materials. Any of these techniques could provide a useful estimate of the number of active sites, and the development of new methodologies for this task is still an active area of research, for MoS_2 as well as for other electrocatalyst materials for the HER and other reactions.

In summary, measuring the total active surface area is the most common strategy for determining the number of active sites on many electrocatalysts and there exist many effective methods for doing so. For MoS_2 materials techniques that specifically determine the number of active edge sites are particularly helpful. Counting the number of active sites is typically easiest for model systems with low catalyst loading. Additional approximations are often necessary for electrodes with high total activity.

3.2.2. Calculating the TOF of Each Site. The activity of each surface site, quantified as the TOF, is generally the most significant factor affecting the overall activity of an electrode for

dx.doi.org/10.1021/cs500923c | ACS Catal. 2014, 4, 3957−3971

the HER, as TOFs can vary by more than 10 orders of magnitude for different electrocatalysts, while the density of surface sites on an electrode typically varies by only up to ~3 orders of magnitude.[91,92] Thus, determining the active site TOF is especially critical in evaluating novel electrocatalyst materials. The TOF is primarily determined by the physical and chemical properties of the catalyst surface that ultimately determine parameters critical to the reaction chemistry at active sites, including the binding energies of reactive intermediates and the activation energies involved in the elementary steps. The TOF, however, is difficult to measure directly, so it is typically inferred from the measurements of total electrode activity and the number of sites as described above. While each unique active site may have a different turnover frequency, there is usually no practical means to measure the TOF of one site in isolation, so reported TOF numbers are almost always averages over many sites.

While it is generally assumed that hydrogen binds to undercoordinated sulfur edges sites, in this perspective, we use the TOF in units of H_2 s^{-1} per surface Mo atom to compare the intrinsic activities of molybdenum sulfide HER catalysts. This avoids difficulties in distinguishing the activity among different sulfur edge sites. A number of different research groups have designed MoS_2 nanostructures with high edge site exposure and electrical accessibility. The surface Mo atom-normalized TOF provides useful insights about the efficacy of these strategies, as it can be used to infer the fraction of surface sites that are active. Another important research aim is to improve the TOF of each active site by modifying the properties of the molybdenum sulfide. Comparing the average TOF of the active sites for such catalysts would be ideal, but the data necessary to make this comparison are not readily available due to variations in the methods used to measure and report active site concentrations as well as differences in catalyst structure and stoichiometry. Performing a consistent comparison of the surface Mo atom-normalized TOF is practical given available data, and though this strategy is not perfect, it still provides useful insights about the intrinsic activity of the modified catalysts.

3.2.3. Complicating Factors. Slow mass transport can complicate the determination of the total electrode activity and active site TOF, but appropriate experimental procedures can usually reduce this effect. For HER catalysts operating in acidic electrolyte, the concentration of protons is typically high enough that diffusion limitations are not encountered, but slow mass transport may become significant in porous electrodes operating at large current densities. Hydrogen bubbles may also accumulate at the electrode surface and block some active area; a rotating disk electrode can often be helpful in this regard.

Electrical series resistance can also impact activity measurements through *iR* potential drops. Experimenters can reduce these effects by measuring the circuit resistance using electrochemical impedance spectroscopy and applying an appropriate correction during or after the experiment. This correction does not account for a nonuniform potential across the active surface if the substrate has a high sheet resistance or if the catalyst possesses a three-dimensional nanostructure that results in a range of charge transport path lengths. Nevertheless, when recognized, these effects can usually be mitigated sufficiently to enable a reasonably accurate TOF determination.

Selectivity and stability are other important considerations in measuring the efficacy of electrocatalysts in general. Measuring the current passed through the electrochemical circuit does not reveal which electrochemical reactions occurred so independent measurements of product concentration are essential, especially for cases such as CO_2 reduction.[93] For most HER catalysts, selectivity measurements are important but generally not as crucial as with other reactions, because in acidic electrolytes, H_2 is the only plausible reaction product from proton reduction that can be produced at a significant rate. Nevertheless, under some circumstances, species other than protons might be reduced. Even the electrode material itself may be cathodically corroded, contributing to the measured Faradaic current. Independent measurements of the evolved H_2 concentration using volume displacement, gas chromatography, or an electrochemical hydrogen detector may be necessary to confirm selectivity. Coulometry measurements also provide a straightforward means of initial HER selectivity determination; that is, if the total charge passed in a particular measurement is orders of magnitude higher than would be required to corrode the catalyst itself, this is strong evidence that most of the current must correspond to the HER.

4. STATE OF THE ART MOLYBDENUM SULFIDE ELECTROCATALYSTS

Recent years have seen many efforts to develop improved molybdenum sulfide HER catalysts in several forms, including crystalline, amorphous, and molecular cluster materials. To accomplish this goal, these studies employ two basic strategies corresponding to the two fundamental factors that determine overall electrode activity. First, the activity can be improved by increasing the number of electrically accessible active sites. This is nontrivial, as one must consider the catalyst nanostructure, which controls the atomic structure of the exposed surface, as well as the conductivity between the active sites and the conductive support. Electron and hole mobility is about 2200 times faster along a basal plane than between sheets,[41] so catalytic activity may be hindered if the active sites are separated from the conductive substrate by MoS_2 basal planes oriented parallel to the surface of the support.[76] Second, the activity can also be improved by increasing the TOF of each individual site by modifying the physical or chemical properties of the molybdenum sulfide through surface structure doping, strain, support interactions, or other effects. Herein, we briefly review some recent results in state- of-the-art molybdenum sulfide electrocatalyst design in the context of these activity enhancement strategies. Broadly, we classify these catalysts as crystalline MoS_2 materials, amorphous molybdenum sulfide films, or molecular molybdenum sulfide clusters.

4.1. Crystalline MoS_2. Most recent works on crystalline MoS_2 catalysts have focused on creating device-ready structures by controlling the catalyst nanostructure to increase the number of accessible edge sites per geometric area. MoS_2 morphologies with high active site densities such as nanowires, nanoparticles, and modified thin films have all been developed. The materials discussed in this section have a 2H polymorph hexagonal crystal structure and are synthesized primarily through gas phase sulfidization of a molybdenum-containing precursor (molybdenum metal or molybdenum oxide) or by hydrothermal methods.[38,54,58,59,63]

4.1.1. MoS_2 Nanowires. MoS_2−MoO_3 core−shell nanowires, as seen in Figure 6, were synthesized by sulfidizing MoO_3 nanowires in a 10% H_2S/90% H_2 atmosphere.[54] This nanowire morphology was developed for its high surface area, which gives it the potential to expose a large number of active edge sites per geometric electrode area. Furthermore, the conductive MoO_3

dx.doi.org/10.1021/cs500923c | ACS Catal. 2014, 4, 3957−3971

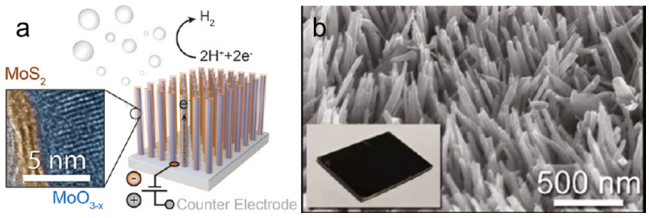

Figure 6. (a) TEM image of MoS_2/MoO_{3-x} shown structurally (right). This catalyst shows no degradation after 10 000 potential cycles despite the fact that MoO_3 is unstable in acid and only three layers (2−3 nm) of MoS_2 protect it. (b) SEM image of MoS_2/MoO_{3-x} nanowires after 200 °C thermal sulfidization. The inset shows a photograph of the sulfidized sample. Reproduced with permission.[54]

core facilitates charge transport along the length of the nanowires, improving the electrical accessibility of the active sites. This catalyst possessed reasonably high HER activity, achieving 10 mA/$cm^2_{electrode}$ at 250 mV overpotential. However, the surface Mo-atom averaged TOF determined using anodic stripping of the MoS_2 and TEM imaging revealed a low density of exposed active edge sites, as the MoS_2 basal planes curved around the circumference of the nanowires. This result emphasizes one particular strategy to improve overall activity, designing the nanoscale morphology of the MoS_2 to favor higher exposure of active edge sites rather than extended basal planes, a valuable insight for further catalyst design efforts.

The outstanding stability of MoS_2 in acidic electrolyte was another key insight provided by this structure. The thickness of the MoS_2 shell was shown to depend on sulfidization temperature. At the lowest temperature tested, 150 °C, the sulfidation was incomplete, leaving a shell with pinholes exposing the acid-unstable MoO_3 cores and causing rapid degradation during potential cycling. Sulfidization at 200 °C produced a MoS_2 shell ∼3 nm thick, and was found to have the highest HER activity among the samples investigated. This sample lost no activity over 10 000 potential cycles in 0.5 M H_2SO_4, demonstrating the ability of MoS_2 to withstand very harsh testing conditions while protecting the underlying MoO_3 core, a key asset for practical device integration

4.1.2. Mesoporous Double Gyroid MoS_2. The double gyroid mesoporous nanostructure, shown in Figure 7, exhibits a high surface area despite minimal total film thickness.[58] The double gyroid is an excellent structure for a MoS_2 HER catalyst because its nanoscale curvature mitigates the formation of extended basal planes, resulting in a high density of exposed active edge sites. This MoS_2 structure was synthesized by electrodepositing MoO_x in a silica double gyroid template, sulfidizing the MoO_x in 10% H_2S/90% H_2 at 200 °C, and removing the silica template with a hydrofluoric acid etch. The resulting catalyst showed improved activity, achieving 10 mA/$cm^2_{electrode}$ at 220 mV overpotential. The electrochemically active surface area of this structure was determined using capacitance measurements, and the resultant surface Mo-atom averaged TOF showed that the fraction of active sites exposed at the surface of the double gyroid was 2−4 times higher than in the MoO_3−MoS_2 nanowires. An additional advantage of the MoS_2 double gyroid is its tunable thickness. If MoS_2 catalysts are to be integrated into cost-effective PEC water splitting devices, synthesizing highly active thin film structures that do not absorb a large portion of incoming solar radiation is desirable. The double gyroid film thickness is tunable by varying the MoO_x electrodeposition time, allowing for a trade-

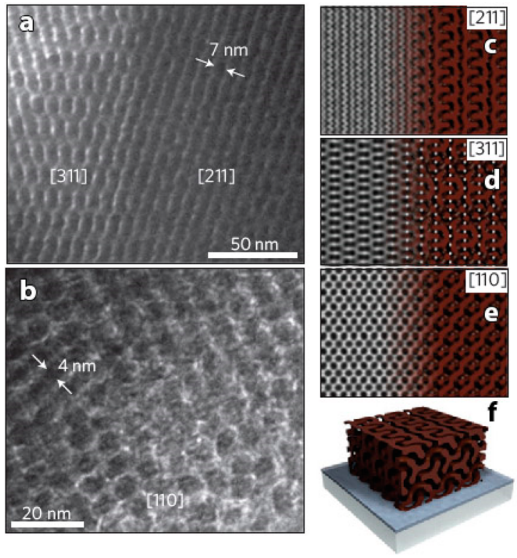

Figure 7. MoS_2 double gyroid mesoporous structure. (a) TEM image of the [311] and [211] projections. (b) TEM image of the [110] projection. (c−e) Models corresponding to simulated TEM images of the [211], [311], and [110] projections, respectively. (f) 3D model of the double dyroid. Reproduced with permission.[58]

off between thicker films that have higher activity and thinner films that have lower parasitic light absorption. A downside of the MoS_2 double gyroid is an increase in resistive losses due to long path lengths for electron transport from the active site to the conducting or semiconducting substrate.

4.1.3. MoS_2 Nanoparticles. MoS_2 nanoparticles have been synthesized a variety of ways, including chemical exfoliation of a MoS_2 precursor,[94] thermal sulfidization of heptamolybdate precursor,[52,95] and chemical reduction of MoS_3 nanoparticles.[72] Various optimal loadings and activities were reported, likely resulting from various degrees of success with nanoparticle dispersion. Highly dispersed nanoparticles will allow access to more active sites than agglomerated particles. As shown in Figure 8, the most active electrodes to date based on MoS_2 nanoparticles were synthesized on reduced graphene oxide (RGO) nanosheets to increase the amount of active edge sites per geometric surface area. Solvothermal synthesis was carried out using $(NH_4)_2MoS_4$ and hydrazine in dimethylformamide at 200 °C. Coupling MoS_2 nanoparticles with the RGO support showed a substantial improvement in activity compared to free MoS_2 nanoparticles. The RGO support led to better nanoparticle dispersion and a different morphology compared to the agglomerated RGO-free nanoparticles. These differences ultimately led to superior active site access and likely better charge transport from the active site to the glassy carbon disk or porous carbon paper onto which the catalyst was loaded for testing. The Tafel slope was 41 mV/decade, in line with the best Tafel slopes ever reported for MoS_2 catalysts,[69,96] and the catalyst achieved 10 mA/$cm^2_{electrode}$ at ∼150 mV overpotential. The high total electrode activity of these catalysts was due in large portion to a very high catalyst loading (1 mg/$cm^2_{electrode}$).[63] More recent work has shown that MoS_2 has also been combined with other carbon nanomaterials to form very active electrodes.[64,65]

4.1.4. Vertically Aligned MoS_2 Thin Films. In an effort to expose a high density of edge sites and reduce resistive losses from electron transport perpendicular to MoS_2 basal planes, Kong et al. synthesized vertically aligned crystalline MoS_2.[59]

dx.doi.org/10.1021/cs500923c | ACS Catal. 2014, 4, 3957−3971

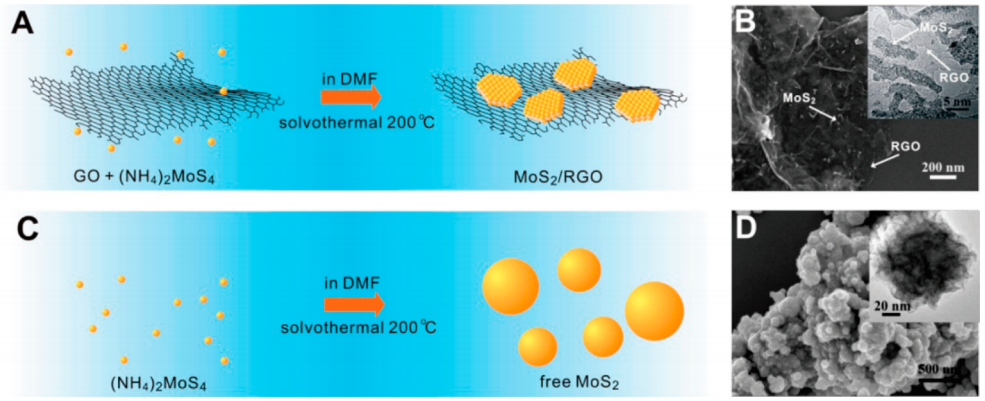

Figure 8. Synthesis of MoS_2 nanoparticles with and without reduced graphene oxide (RGO) sheets. (a) Schematic diagram of MoS_2/RGO nanoparticle synthesis. (b) SEM and inset TEM images of the MoS_2/RGO catalyst. (c) Schematic of large, free MoS_2 nanoparticle synthesis. (d) SEM and inset TEM images of the MoS_2 particles with no RGO. Reproduced with permission.[63]

The vertically aligned MoS_2, shown in Figure 9, exposes primarily edge sites to the electrolyte and allows fast electron transport through a single MoS_2 layer to the conducting substrate. Synthesis is achieved by exposing a 5 nm electron beam evaporated Mo film to 100 mTorr elemental sulfur vapor for 10 min at 550 °C, a sulfurization temperature later found to produce active MoS_2 nanosheets.[59,97] The vertically oriented catalyst morphology is promising because MoS_2 with only exposed edge sites should increase the number of active sites available to perform HER. The exchange current density of 2.2×10^{-6} A/cm$^2_{electrode}$ is high and corresponds to a TOF of about 0.013 s^{-1} but the Tafel slope is also rather high (120 mV/decade). By extrapolation, the 10 mA/cm$^2_{electrode}$ is reached at 440 mV overpotential, resulting in a comparatively low catalyst activity on a geometric basis. However, these films show an exciting new geometry and may make extremely active catalysts if nanostructured or loaded on a higher surface area support.[59]

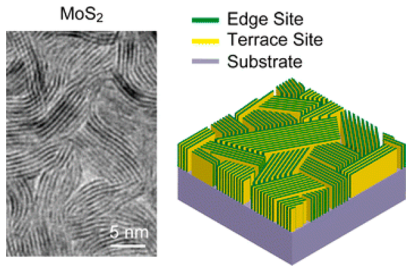

Figure 9. Vertically aligned MoS_2 sheets. TEM image (left) and schematic diagram (right) indicating edge sites and terrace sites. Reproduced with permission.[59]

4.2. Amorphous Molybdenum Sulfides. Amorphous molybdenum sulfides have been known for several decades,[98−104] but their excellent catalytic activity for the HER was discovered only recently.[50,69,70,72,73,105] These materials can be synthesized using electrodeposition or wet chemical reactions with no thermal sulfidization treatment, which may make them particularly advantageous for some applications.[50,69,70,72] This material has been successfully applied in several photoelectrochemical and photocatalytic water splitting devices.[106−108]

Amorphous molybdenum sulfide catalysts often possess high overall electrode activities, largely due to their high surface area morphologies.[50,69,70,72,73] Amorphous MoS_x catalysts that achieved 10 mA/cm$^2_{electrode}$ at −0.20 V versus RHE were measured to have roughness factors of nearly 100, corresponding to a total surface site density on the order 10^{17} per cm$^2_{electrode}$ and a resulting TOF around 0.3 H_2 s^{-1} per site averaged over the total surface.[50] Physical and chemical characterization have revealed that as synthesized, the amorphous material typically possesses a composition close to MoS_3, but upon applying a cathodic potential, the surface composition changes to MoS_2.[50,69,72] Thus, the electrochemically active surface likely resembles crystalline MoS_2 in chemical state, though no studies to date have shown evidence of crystallinity in this material. While it is difficult to identify the specific active sites on amorphous molybdenum sulfide surfaces due to their significant atomic-scale heterogeneity, these results

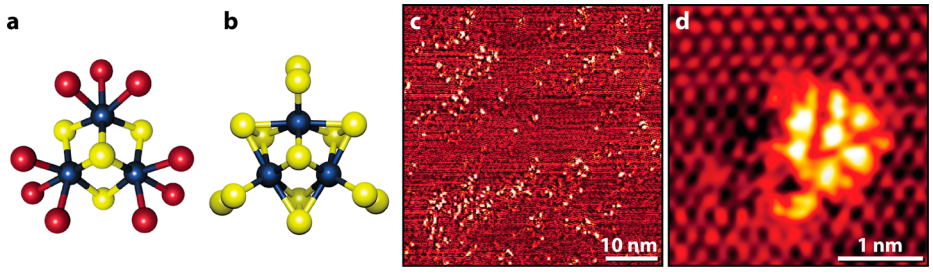

Figure 10. (a,b) Structure of $[Mo_3S_4]^{4+}$ cubane and $[Mo_3S_{13}]^{2-}$ nanoclusters, respectively. Blue: Mo atoms, yellow: S atoms, and red: O atoms (from water ligands). (c) STM image of anodized HOPG surface after drop-casting $[Mo_3S_{13}]^{2-}$ clusters. (d) Atom-resolved STM image of a single $[Mo_3S_{13}]^{2-}$ cluster. Reproduced with permission.[55,96]

dx.doi.org/10.1021/cs500923c | ACS Catal. 2014, 4, 3957−3971

suggest that the active sites probably have similar TOFs to those observed on the edges of crystalline MoS_2.

4.3. Molybdenum Sulfide Molecular Clusters. Molybdenum sulfide nanocluster compounds that bridge molecular and solid-state electrocatalysis when supported on electrode surfaces are another interesting class of HER catalysts. These inorganic clusters consist of small molecular units of molybdenum sulfide with undercoordinated sulfur abounding at its surface, resembling MoS_2 edges. Two examples, the incomplete $[Mo_3S_4]^{4+}$ cubane and the thiomolybdate $[Mo_3S_{13}]^{2-}$ nanocluster, are shown in Figure 10.

The incomplete $[Mo_3S_4]^{4+}$ cubanes have been demonstrated to be active for electrocatalytic and photoelectrochemical hydrogen production.[55,109] STM images of HOPG-supported $[Mo_3S_4]^{4+}$ cubanes showed that individual clusters were uniformly scattered on the HOPG surface and the surface coverage was determined to be 1.0 ($\pm$0.1) $\times$ 10^{13} clusters/cm^2. Together with an exchange current density of 2.2 $\times$ 10^{-7} A/cm$^2_{electrode}$, this surface coverage yielded a TOF per $[Mo_3S_4]^{4+}$ cluster of 0.07 s^{-1} at 0 mV overpotential. However, the hydrophilicity of the cubanes made the activity decrease over time due to desorption of the catalyst.[55] This was largely mitigated, provided that the concentration of O_2 was kept low ($\leq$15 ppb) in the system, in a later photoelectrochemical study by changing to methylcyclopentadienyl ligands to obtain less hydrophilic clusters and avoid deactivation by dissolution of the hydrophilic cubanes.[109]

Recently, thiomolybdate $[Mo_3S_{13}]^{2-}$ nanoclusters have also been examined for the HER. These clusters are prepared by straightforward wet chemical methods and can be supported on a variety of substrates by simple drop-casting from a methanol solution. Similar to the $[Mo_3S_4]^{4+}$ cubanes, the $[Mo_3S_{13}]^{2-}$ nanoclusters were supported on anodized HOPG and imaged with STM. The surface coverage of $[Mo_3S_{13}]^{2-}$ clusters was determined to be ~8 ($\pm$2) $\times$ 10^{12} $[Mo_3S_{13}]^{2-}$ clusters per cm^2 HOPG. These HOPG supported $[Mo_3S_{13}]^{2-}$ clusters showed the highest HER turnover frequency of any molybdenum sulfide catalyst ever synthesized by scalable wet-chemical methods (see section 5.1). Furthermore, the $[Mo_3S_{13}]^{2-}$ clusters have very low solubility in water[110] and show better stability at similar current densities than the hydrophilic $[Mo_3S_4]^{4+}$ cubanes.

4.4. Stability of Molybdenum Sulfides. Catalyst stability is an important, but often overlooked, aspect of device-oriented electrocatalysts. The fuel cell research field has adopted standard methods for accelerated durability tests that apply to fuel cell membrane electrode assemblies,[111] but no such standard protocols exist for catalysts in electrolyzers or photoelectrochemical water splitting devices, where MoS_2 electrocatalysts might be utilized. In the MoS_2 electrocatalysis literature, potential cycling has been the predominant method used to assess catalyst stability. Simplistically, potential cycling approximates startup-shutdown conditions in an electrolyzer and illumination intensity fluctuations in photoelectrochemical devices and in principle can provide a harsher and faster way to examine stability than with either chronoamperometry (constant potential) or chronopotentiometry (constant current) testing. However, it may also be beneficial to perform constant current or potential measurements which may better simulate long-term operation conditions. Photoelectrochemical device degradation testing is further complicated by illumination conditions. The true potential at the semiconductor surface is related to both the applied potential and the photovoltage, a fact that must be accounted for when testing illuminated photoelectrodes.

Crystalline MoS_2 materials have typically demonstrated greater stability than amorphous and molecular MoS_2 catalysts. A commonly used protocol to access stability is 1000 potential cycles, though various scan rates and potential ranges have been employed in various works.[59,63,94] Nevertheless, all these catalysts showed negligible or near-negligible loss in activity after cycling. Intense stability testing of 10 000 potential cycles between +0.2 and −0.3 V vs RHE at 50 mV/s was conducted on the MoO_3−MoS_2 nanowires, which showed no measurable activity loss, highlighting the exceptional stability of crystalline MoS_2.[54] Amorphous MoS_x, though not as stable as crystalline MoS_2, still exhibits reasonable stability. The potential to achieve 10 mA/cm$^2_{electrode}$ increased by only 57 mV after 10 000 potential cycles from +0.1 V to −0.25 V vs RHE at 50 mV/s; 30 mV of which was recovered by simply refreshing the electrolyte.[50] The molecular cluster catalysts were the least stable form of molybdenum sulfide. The $[Mo_3S_4]^{4+}$ cubanes on Vulcan XC-72 carbon black lost significant activity between the first and tenth potential cycle as the overpotential to reach 10 mA/cm$^2_{electrode}$ dropped from about −240 mV to −270 mV.[55] This activity loss was attributed to catalyst desorption. The $[Mo_3S_{13}]^{2-}$ cluster catalyst has excellent stability for a molecular catalyst, only increasing by 13 mV overpotential required to achieve 10 mA/cm$^2_{electrode}$ from −0.187 mV vs RHE to −0.200 mV vs RHE after 1000 potential cycles.[96] However, the Mo_3S_{13} was supported on carbon paper so the interaction between the catalyst and support may be different than that between cubanes and carbon black, which could account for the measured stability differences. In both cases, desorption is likely the primary cause of the observed activity loss.

4.5. Emerging Directions. Most of the emerging directions in molybdenum sulfide research involve increasing overall edge site turnover frequency, inspired in large part by past successes in MoS_2 research reported in the hydrodesulfurization (HDS) literature, a field in which carbon and alumina supported MoS_2 has long been an economically viable catalyst.[112−115] This reciprocity is not surprising because an active HDS catalyst must also bond hydrogen when removing sulfur as H_2S from refined petroleum products. Four novel approaches in improving the intrinsic activity of MoS_2 are activating the S-edge by doping, modifying the H-binding energy through substrate interactions, tuning electronic properties through Li^+ ion intercalation, and utilizing the conductive 1T polymorph of MoS_2.

4.5.1. Doping. It has been well-established that adding small amounts of transition metal dopants including Co and Ni to MoS_2 can increase its catalytic activity for HDS by more than an order of magnitude.[116−119] Studies using STM have revealed that these dopants are located predominantly at the S-edges of doped MoS_2 clusters, and that the activity enhancements arise from the dopant's role in modifying the hydrogen bonding energy at the S-edges.[120] Similar to the HDS reaction, doping with Fe, Co, and Ni has also been demonstrated to increase the HER activity of the MoS_2 S-edge.[52,70,121] DFT calculations showed that in unmodified MoS_2, the hydrogen binding energy, ΔG_H, is 0.08 eV at the Mo-edge and 0.18 eV at the S-edge. Incorporating Co dopants decreased the binding energy at the S-edge from 0.18 to 0.10 eV, while the ΔG_H at the Mo-edge was unaffected. Hence, the role of Co is to increase the number of active sites in nanostructured MoS_2 catalysts by activating the S-edges. Thus, while these studies have demonstrated

dx.doi.org/10.1021/cs500923c | ACS Catal. 2014, 4, 3957−3971

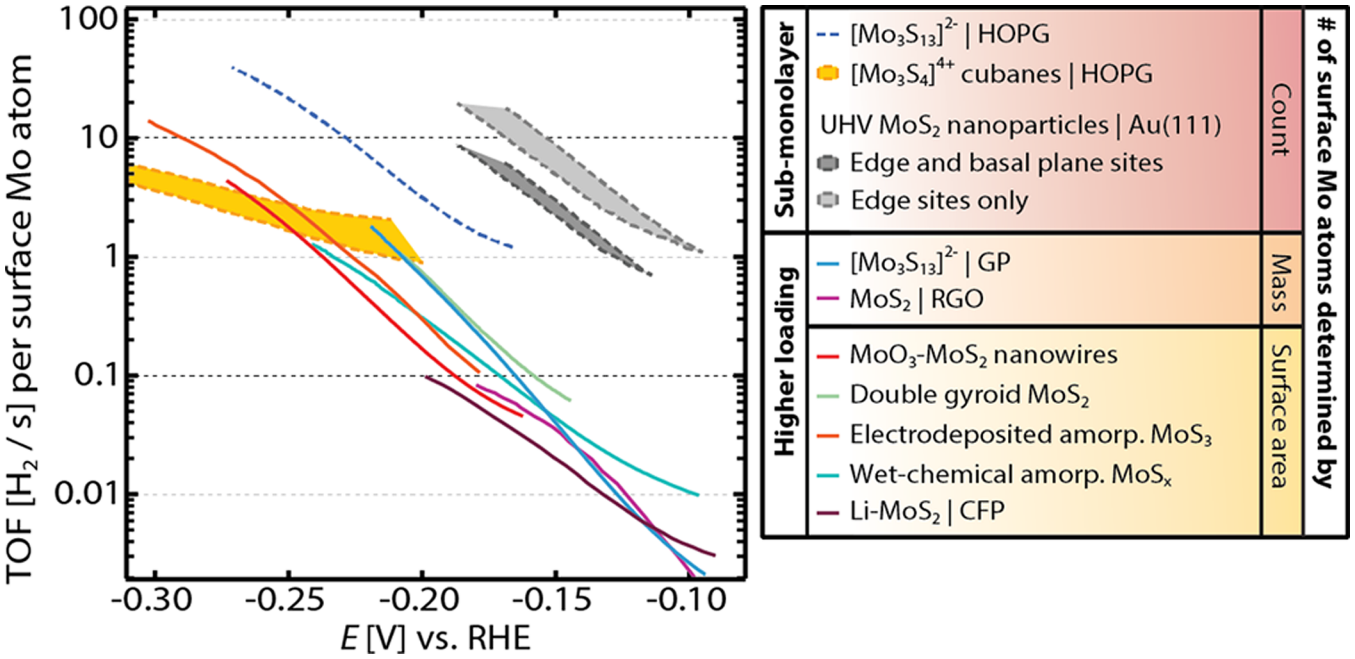

Figure 11. Turnover frequencies of different molybdenum sulfide catalysts normalized to the number of surface Mo atoms.

important activity enhancements, greater gains may be possible if the ΔG_H at the active sites even can be reduced even further to approach 0.00 eV using new doping strategies.

Transition-metal dopants including Ni, Co, and Fe have also been used to improve the activity of amorphous molybdenum sulfide catalysts.[70] Cobalt doping was most successful, yielding changes in the catalyst morphology that increased the active surface area more than 300%, resulting in electrodes that achieved 10 $mA/cm^2_{electrode}$ at −0.17 V vs RHE in pH 0 electrolyte.[70] Under these conditions, the doping did not affect the intrinsic activity of the catalyst, but the doping did improve the per-site TOF in pH 7 electrolyte.

Doping MoS_2 with other transition metals to make mixed metal sulfides may also provide a promising path to higher HER activity. $Mo_{1-x}V_xS_2$ catalysts ($x \sim 0.05$) were shown to be more active for hydrogen evolution than similarly prepared MoS_2.[122] The activity enhancement resulted from lower resistivity and higher carrier concentrations. Further efforts to understand the effects of doping this material may enable additional improvements in its performance.

4.5.2. Substrate Interactions. Theoretical results from density functional theory have also predicted that H-binding at both the edge sites and the basal plane of single layered MoS_2 could be modified by support interactions, and thereby tune HER activity.[123,124] The change in hydrogen binding is shown to arise from support interactions involving van der Waals forces. Stronger adhesion of the MoS_2 onto the support leads to weaker hydrogen binding, which may yield several orders of magnitude difference in HER turnover frequency. These results may explain the lower than expected exchange current densities of supported MoS_2 in electrochemical H_2 evolution studies compared to theoretical predictions.[123] It may be possible to optimally tune the hydrogen binding with a support that binds MoS_2 with a physisorption strength of approximately −0.30 eV.[123]

4.5.3. Li Intercalation. Intercalation of Li ions into the van der Waals gaps tunes the electronic properties of MoS_2, which leads to an increase in HER activity.[14,67,71,75] The Li electrochemical intercalation was explained to have at least three effects on the electronic structure of MoS_2.[75] First, Li ions change the electronic band structure by increasing the layer spacing and eventually exfoliating MoS_2 into individual layers. Second, the intercalated Li could change the d-band filling and reduce the oxidation state of Mo. This could significantly change the H-binding energy and improve the HER activity. Third, high Li content leads to a phase transition for MoS_2 from the 2H semiconducting phase to the 1T metallic phase, which could lead to an increase in conductivity of the catalyst and potentially activate the inactive basal plane, as discussed further below.[71,75] Li intercalation was applied to vertically aligned MoS_2 on high surface area carbon substrates deposited by atomic layer deposition of MoO_3 followed by rapid sulfurization. This catalyst demonstrated an impressively low overpotential of 168 mV at 10 $mA/cm^2_{electrode}$ and negligible degradation after 1000 cycles.[75]

4.5.4. 1T Phase of MoS_2. Exfoliation of flowerlike MoS_2 nanostructures was demonstrated using a reaction of *n*-butyllithium and water, yielding metallic 1T-phase MoS_2 nanosheets.[67] These polymorph catalysts required only 187 mV to reach 10 $mA/cm^2_{electrode}$, surpassing the activity of similarly prepared 2H-phase catalysts by 130 mV. Lukowski et al. argue that this is achieved by increasing the number of active edge sites and drastically improving the charge transfer resistance from 232 Ω to only 4 Ω. In another study by Voiry et al., the origin of active sites on 1T-phase MoS_2 nanosheet was investigated by partially oxidizing both bulk 2H-phase MoS_2 and MoS_2 nanosheets.[71] It was shown that the activity of 2H-phase MoS_2 was significantly reduced after oxidation, presumably due to the oxidation of the edge sites. On the other hand, the 1T-phase MoS_2 remains unaffected after oxidation. Voiry and co-workers suggested that edges of the 1T-phase MoS_2 nanosheets are not the main active sites and the basal plane could be catalytically active.[71] A recent catalyst consisting of Li^+-intercalated 1T-phase MoS_2 on a high surface area carbon fiber paper demonstrated excellent total electrode

dx.doi.org/10.1021/cs500923c | ACS Catal. 2014, 4, 3957−3971

activity, with a current density of 10 mA/cm$^2_{electrode}$ achieved at 110 mV overpotential.[81]

5. COMPARISON OF MOS_2 CATALYSTS

As discussed in Section 3, in this review, we focus on two metrics for comparing the HER activity of the different molybdenum sulfide catalysts: intrinsic activity as measured by TOF per surface exposed Mo atom and total electrode activity measured by the potential to reach a current density of 10 mA/cm$^2_{electrode}$.

5.1. Intrinsic Activity. For 2H-phase MoS_2 it is well-established that the (0001) basal planes are catalytically inert,[35] whereas only undercoordinated sulfur atoms at the edges are active. However, given the myriad of different S possible terminations in various state-of-the-art molybdenum sulfide catalysts, we have found previously that calculating the TOF per surface Mo atom (as opposed to S atom) can help facilitate the direct comparison of different catalyst materials.[96]

The TOF plot in Figure 11 shows that all forms of nanostructured molybdenum sulfides exhibit high catalytic activity for the HER. On a TOF basis, the most active molybdenum sulfide HER catalyst ever reported consists of UHV-deposited MoS_2 nanoparticles on Au(111) substrates.[36] The edge sites of these MoS_2 nanoparticles exhibit TOFs (per edge site) of 1 s^{-1} and 10 s^{-1} at overpotentials of approximately 0.10 and 0.16 V, respectively.[36] This sets the benchmark for HER catalysis on MoS_2. For comparison, Pt catalysts have exchange current densities in the range of 0.4−400 mA/cm^2.[47,125] These values correspond to exchange TOF values on the order of 1−1000 H_2/s per site at 0 V overpotential.[47,125] The TOF values for Pt reported previously vary over this wide range due to differences in the platinum preparation and measurement techniques employed.[125] The extremely high activity of platinum makes it difficult of measure the TOF without influence of transport limitations, and under the carefully controlled conditions necessary to measure the TOF accurately the Pt electrodes are typically not biased to potentials negative of −0.10 V vs RHE.[125] Therefore, while it is difficult to directly compare the TOF values of Pt and MoS_2 at the same overpotential, these results indicate that the intrinsic activity of Pt is approximately $10^2 - 10^5$ times greater than that of MoS_2 edges.

The intrinsic activity of other molybdenum sulfides typically falls 1−2 orders of magnitude below that of the UHV-prepared nanoparticles. The highest activity of a molybdenum sulfide prepared by a scalable route is found for a submonolayer of $[Mo_3S_{13}]^{2-}$ clusters on an HOPG crystal. The high TOF recorded for these two particular systems, MoS_2 nanoparticles on Au(111) and $[Mo_3S_{13}]^{2-}$ clusters on HOPG, may be due in large part to their submonolayer coverage, where mass transport and electrical accessibility are at a maximum.

5.2. Total Electrode Activity. Whereas TOF is the best figure of merit when comparing the intrinsic catalytic activity of a material, total electrode activity is useful to consider from a practical, device oriented point of view. For the HER, it is useful consider the potential necessary to reach a current density of 10 mA/cm$^2_{electrode}$ electrode, as discussed in section 3.1.

Figure 12 shows the LSV of different molybdenum sulfide materials and sample architectures.[50,54,58,62,63,69,71,75,81,96,126] Not surprisingly, the trend in Figure 12 shows that electrodes with very high catalyst loadings generally have the highest overall activity. On a geometric area basis, electrodes with the highest demonstrated activity include: MoS_2 nanoparticles on reduced graphene oxide,[63] MoS_x on piranha etched graphite paper,[62] and $[Mo_3S_{13}]^{2-}$ clusters on electrochemically anodized graphite paper (this work), all of which require an overpotential of approximately 150 mV to reach 10 mA/cm$^2_{electrode}$. Two electrodes that each require only 110 mV overpotential to reach 10 mA/cm$^2_{electrode}$ were recently reported.[81,126] The first was composed of amorphous MoS_x on nitrogen-doped carbon nanotubes, whereas the second consisted of Li^+-intercalated 1T-phase MoS_2 on carbon fiber paper. These electrode possess the highest geometric area-normalized activity reported to date. This activity is very impressive, indeed, in particular because molybdenum sulfides are earth-abundant, nonprecious metal catalysts with demonstrated stability in acid.

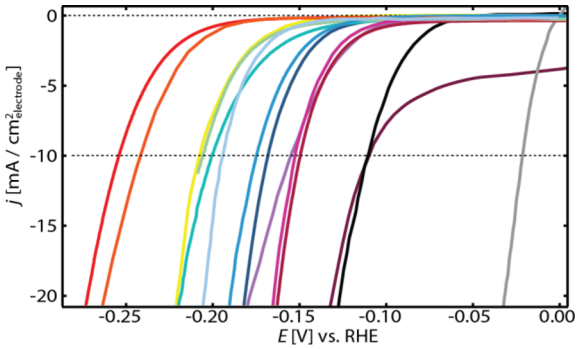

	Reference	Potential for 10 mA/cm$^2_{geo}$ [V] vs. RHE
MoO_3-MoS_2 nanowires	[54]	-0.254
Electrodeposited amorp. MoS_3	[69]	-0.242
1T - MoS_2	[71]	-0.207
Double gyroid MoS_2	[58]	-0.206
Wet-chemical amorp. MoS_x	[50]	-0.200
MoS_x | GP	[62]	-0.194
100 μg/cm^2 $[Mo_3S_{13}]^{2-}$ | GP	[96]	-0.174
Li_xMoS_2 | GP	[75]	-0.168
MoS_2 | RGO	[63]	-0.154
MoS_x | Piranha GP	[62]	-0.152
$[Mo_3S_{13}]^{2-}$ | anodized GP	This work	-0.149
Li-MoS_2 | CFP	[81]	-0.110
MoS_x | N-CNT	[126]	-0.110
Polycrystalline Pt	This work	-0.021

Figure 12. Linear sweep voltammograms demonstrating the total electrode activity different molybdenum sulfide catalysts. The potential required to reach a current density of −10 mA/cm$^2_{electrode}$ is reported to the right. Polycrystalline Pt is shown for comparison.

6. APPLICATIONS

6.1. Molybdenum Sulfide in Photoelectrodes. Molybdenum sulfide HER catalysts have been successfully applied in a number of photoelectrochemical devices. Early research focused on bulk MoS_2 crystals as full photoelectrodes where the MoS_2 acts as both light absorber and catalyst, but to date, these devices have shown poor performance for hydrogen production.[35,127−133] A recent study suggests that MoS_2 photocathodes may be inherently limited because the catalytically active edge sites may also serve as recombination centers.[77] It may be possible to overcome this trade-off with further research on surface engineering strategies.

Nevertheless, molybdenum sulfides have been successfully employed as the HER catalyst in combination with other semiconductor light absorbers for photocatalytic and photoelectrochemical water splitting.[76,106,107,109,134−148] In particular, recent studies have shown that combining MoS_2 with silicon can yield highly active complete water splitting photocathodes.[106,149] In this system, the catalyst must possess high

dx.doi.org/10.1021/cs500923c | ACS Catal. 2014, 4, 3957−3971

activity for the HER while exhibiting minimal light absorption. The silicon surface must also be protected to prevent corrosion or oxidation in an aqueous electrolyte. To this end, a conformal layer of MoS_2 on the Si photoelectrode surface can function as a protecting layer while simultaneously catalyzing the HER. The flat MoS_2 layers possessed only moderate HER activity because of the low density of active sites exposed at the photocathode surfaces, but the activity of the photocathodes was increased by adding amorphous molybdenum sulfide or $[Mo_3S_{13}]^{2-}$ clusters to increase the HER active site density.[106,149] One drawback of these electrode designs is that the saturation photocurrent density is limited by undesired parasitic light absorption in the molybdenum sulfide layers. With further effort, molybdenum sulfide/silicon photocathodes could potentially match the performance achieved using platinum.

6.2. Acid Electrolyzers. Alkaline electrolyzers and polymer electrolyte membrane (PEM) eletrolyzers are the two main types of commercially available low temperature (<100 °C) water electrolyzers.[23] Alkaline electrolyzers use nonprecious nickel-based catalysts and an aqueous KOH electrolyte with a diaphragm separating the electrode compartments.[23] Commercial PEM electrolyzers use precious metal Pt and Ir catalysts with a solid proton transporting electrolyte membrane, typically Nafion, between the electrodes.[150] Though unexplored in the literature, MoS_2 may have a future niche as a nonprecious alternative to Pt catalysts for PEM electrolyzer cathodes.

Alkaline electrolyzers are the industry standard for water electrolysis due to their nonprecious metal catalyst utilization and durable design.[151] Though they are currently more expensive, PEM electrolyzers are superior to alkaline electrolyzers in a variety of ways which may lead to their broader implementation.[19] Using an aqueous KOH electrolyte in a conventional alkaline electrolyzer means that the cell cannot be pressurized and it can slowly acidify over time due to atmospheric CO_2. The diaphragm that separates electrode compartments can also allow unwanted hydrogen crossover into the oxygen compartment. The combination of liquid electrolyte and diaphragm also lead to high ohmic losses which limit the maximum operating current density.

PEM electrolyzers, which typically use Nafion polymer electrolyte membranes, can be pressurized, potentially negating the need for an external compressor, have low reactant crossover, and run at higher current densities due to faster electrode kinetics and higher ion conductivity.[19,152] One of the major downsides of conventional PEM acid electrolyzers is their use of precious metal catalysts, which are the most active known acid-stable HER catalysts. Typically platinum is used as a cathode catalyst and iridium is used as an anode catalyst. Currently, the catalyst costs of PEM electrolyzers are a small fraction of the total capital costs,[150] but as the prices of the other electrolyzer stack components decrease, replacing Pt will yield greater fractional cost savings. Additionally, the scarcity of Pt could hinder the scale-up of PEM electrolyzers to the TW scale; approximately 400 000 kg Pt, roughly equivalent to the entirety of global Pt production over 2 years,[153] would be required to implement 1 TW of total electrolyzer capacity assuming 0.5 mg/cm^2 platinum loading and operating current densities of 1 A/cm^2. Developing a means to minimize or avoid Pt in PEM electrolyzers could help enable scale-up of this technology in the future. Ir also suffers from the same scarcity problems as Pt and a nonprecious metal alternative oxygen evolution catalyst must also be found to enable PEM electrolyzer scale-up.[153]

MoS_2 and related materials are good candidate nonprecious metal HER catalysts that could be used in PEM electrolyzers, as they are both active and stable in acid, especially if further research leads to even more active catalyst formulations that can compete with platinum. To our knowledge, no one has reported a true PEM electrolyzer which uses MoS_2 as the cathode catalyst to evolve hydrogen. However, MoS_2 catalysts loaded on gas diffusion electrodes have shown high activity.[154] New metrics will likely be necessary to evaluate MoS_2 catalysts intended for use in PEM electrolyzers: the 10 mA/cm^2 total electrode activity metric discussed in this work is not suitable because electrolyzers operate at approximately 1 A/cm^2 current densities.[19] Other performance metrics may also become more important. For example, a low Tafel slope, good catalyst adhesion to the conductive support under vigorous bubbling, and effective mass transport through the electrode structure will likely be essential for high current operation. Given the present state of high performance molybdenum sulfide catalysts, the future appears bright in terms of developing gas-diffusion electrodes and water electrolyzer systems that incorporate these catalyst materials. For such studies, it is imperative that the electrodes reach current densities on the order of 1 A/cm^2 in order to make for more direct comparisons to Pt-based cathodes designed for implementation in PEM electrolyzers.

7. CONCLUSION

Molybdenum sulfide is an exceptional HER catalyst if it is appropriately nanostructured to expose a high density of active edge sites. We describe two main metrics, total electrode activity and intrinsic active site activity. Both are important in evaluating different catalysts to gain a fundamental understanding of the origins of catalysis as well as to compare activity among candidate materials for device integration. We make the comparisons for intrinsic activity and overall electrode activity for several classes of molybdenum sulfide catalysts, including crystalline MoS_2, amorphous molybdenum sulfide films, and molecular molybdenum sulfide clusters. We describe a number of approaches to engineer molybdenum sulfides to improve their intrinsic activity, pathways that may allow the material to approach the near-ideal HER activity of Pt. Finally, we describe possible applications for MoS_2 in water splitting, by means of water electrolyzers and photoelectrochemical (PEC) cells. Such technologies can help enable more sustainable approaches to energy production, storage and use, particularly involving intermittent renewable energy resources such as wind and solar. Given the importance of lowering the cost of such technologies to be able to compete against fossil fuels, molybdenum sulfide could play an important role as a leading scalable, nonprecious metal catalyst for hydrogen production.

AUTHOR INFORMATION

Corresponding Author

*E-mail: jaramillo@stanford.edu. Tel.: 650-498-6879.

Author Contributions

†J.D.B. and T.R.H. contributed equally to this work

Notes

The authors declare no competing financial interest.

■ ACKNOWLEDGMENTS

This work was supported as part of the Center on Nanostructuring for Efficient Energy Conversion (CNEEC) at Stanford University, an Energy Frontier Research Center funded by the U.S. Department of Energy, Office of Science, Office of Basic Energy Sciences under award no. DE-SC0001060. J.D.B. and T.R.H. acknowledge support from the National Science Foundation Graduate Research Fellowship Program. J.D.B. and P.C. acknowledge Stanford Graduate Fellowships. J.K. acknowledges the Carlsberg Foundation for a postdoctoral fellowship and support from the U.S. Department of Energy, Office of Science, Office of Basic Energy Sciences, under contract no. DE-SC0008685. P.C. was supported by the Assistant Secretary for Energy Efficiency and Renewable Energy, Fuel Cell Technologies Office, of the U. S. Department of Energy under contract number DE-AC02-05CH11231 through subcontract 7058299 from Lawrence Berkeley National Laboratory.

■ REFERENCES

(1) Chu, S.; Majumdar, A. *Nature* **2012**, *488*, 294−303.
(2) *International Energy Outlook 2013*; U.S. Energy Information Administration, U.S. Department of Energy: Washington, DC, 2013.
(3) Lewis, N. S. *Science* **2007**, *315*, 798−801.
(4) Panwar, N.; Kaushik, S.; Kothari, S. *Renewable Sustainable Energy Rev.* **2011**, *15*, 1513−1524.
(5) Solomon, B. D.; Krishna, K. *Energy Policy* **2011**, *39*, 7422−7431.
(6) Solangi, K.; Islam, M.; Saidur, R.; Rahim, N.; Fayaz, H. *Renewable Sustainable Energy Rev.* **2011**, *15*, 2149−2163.
(7) Lim, K. L.; Kazemian, H.; Yaakob, Z.; Daud, W. W. *Chem. Eng. Technol.* **2010**, *33*, 213−226.
(8) Yang, Z.; Zhang, J.; Kintner-Meyer, M. C.; Lu, X.; Choi, D.; Lemmon, J. P.; Liu, J. *Chem. Rev.* **2011**, *111*, 3577−3613.
(9) Walter, M. G.; Warren, E. L.; McKone, J. R.; Boettcher, S. W.; Mi, Q. X.; Santori, E. A.; Lewis, N. S. *Chem. Rev.* **2010**, *110*, 6446−6473.
(10) Abbasi, T.; Abbasi, S. *Renewable Sustainable Energy Rev.* **2011**, *15*, 3034−3040.
(11) Bard, A. J.; Fox, M. A. *Acc. Chem. Res.* **1995**, *28*, 141−145.
(12) Kong, D. S.; Cha, J. J.; Wang, H. T.; Lee, H. R.; Cui, Y. *Energy Environ. Sci.* **2013**, *6*, 3553−3558.
(13) Sobczynski, A.; Yildiz, A.; Bard, A. J.; Campion, A.; Fox, M. A.; Mallouk, T.; Webber, S. E.; White, J. M. *J. Phys. Chem.* **1988**, *92*, 2311−2315.
(14) Voiry, D.; Yamaguchi, H.; Li, J. W.; Silva, R.; Alves, D. C. B.; Fujita, T.; Chen, M. W.; Asefa, T.; Shenoy, V. B.; Eda, G.; Chhowalla, M. *Nat. Mater.* **2013**, *12*, 850−855.
(15) Yang, J.; Shin, H. S. *J. Mater. Chem. A* **2014**, *2*, 5979−5985.
(16) Laursen, A. B.; Kegnæs, S.; Dahl, S.; Chorkendorff, I. *Energy Environ. Sci.* **2012**, *5*, 5577−5591.
(17) Merki, D.; Hu, X. *Energy Environ. Sci.* **2011**, *4*, 3878−3888.
(18) Yan, Y.; Xia, B.; Xu, Z.; Wang, X. *ACS Catal.* **2014**, *4*, 1693−1705.
(19) Carmo, M.; Fritz, D. L.; Mergel, J.; Stolten, D. *Int. J. Hydrogen Energy* **2013**, *38*, 4901−4934.
(20) Holladay, J. D.; Hu, J.; King, D. L.; Wang, Y. *Catal. Today* **2009**, *139*, 244−260.
(21) Zeng, K.; Zhang, D. K. *Prog. Energy Combust. Sci.* **2010**, *36*, 307−326.
(22) Bak, T.; Nowotny, J.; Rekas, M.; Sorrell, C. C. *Int. J. Hydrogen Energy* **2002**, *27*, 991−1022.
(23) Pagliaro, M.; Konstandopoulos, A. G. *Solar Hydrogen: Fuel of the Future*; Royal Society of Chemistry: Cambridge, U.K., 2012.
(24) Doyle, M.; Rajendran, G.; Vielstich, W.; Gasteiger, H.; Lamm, A. In *Handbook of Fuel Cells: Fundamentals, Technology, Applications*; Vielstich, W., Lamm, A., Gasteiger, H. A., Eds; John Wiley & Sons: New York, 2003; Vols. 3 and 4.
(25) McCrory, C. C. L.; Jung, S.; Peters, J. C.; Jaramillo, T. F. *J. Am. Chem. Soc.* **2013**, *135*, 16977−16987.
(26) Kibler, L. A. *ChemPhysChem* **2006**, *7*, 985−991.
(27) Parsons, R. *Trans. Faraday Soc.* **1958**, *54*, 1053−1063.
(28) Nørskov, J. K.; Bligaard, T.; Logadottir, A.; Kitchin, J.; Chen, J.; Pandelov, S.; Stimming, U. *J. Electrochem. Soc.* **2005**, *152*, J23−J26.
(29) Greeley, J.; Stephens, I.; Bondarenko, A.; Johansson, T. P.; Hansen, H. A.; Jaramillo, T.; Rossmeisl, J.; Chorkendorff, I.; Nørskov, J. K. *Nat. Chem.* **2009**, *1*, 552−556.
(30) Greeley, J.; Jaramillo, T. F.; Bonde, J.; Chorkendorff, I.; Nørskov, J. K. *Nat. Mater.* **2006**, *5*, 909−913.
(31) Trasatti, S. In *Advances in Electrochemical Science and Engineering*; Gerischer, H., Tobias, C. W., Eds; Wiley-VCH Verlag GmbH: Weinheim, 2008; *2*, pp 1−85.
(32) Rapoport, L.; Fleischer, N.; Tenne, R. *J. Mater. Chem.* **2005**, *15*, 1782−1788.
(33) Radisavljevic, B.; Radenovic, A.; Brivio, J.; Giacometti, V.; Kis, A. *Nat. Nanotechnol.* **2011**, *6*, 147−150.
(34) Abotsi, G. M.; Scaroni, A. W. *Fuel Process. Technol.* **1989**, *22*, 107−133.
(35) Tributsch, H.; Bennett, J. C. *J. Electroanal. Chem.* **1977**, *81*, 97−111.
(36) Jaramillo, T. F.; Jørgensen, K. P.; Bonde, J.; Nielsen, J. H.; Horch, S.; Chorkendorff, I. *Science* **2007**, *317*, 100−102.
(37) Hinnemann, B.; Moses, P. G.; Bonde, J.; Jørgensen, K. P.; Nielsen, J. H.; Horch, S.; Chorkendorff, I.; Nørskov, J. K. *J. Am. Chem. Soc.* **2005**, *127*, 5308−5309.
(38) Daage, M.; Chianelli, R. *J. Catal.* **1994**, *149*, 414−427.
(39) Winer, W. O. *Wear* **1967**, *10*, 422−452.
(40) Benavente, E.; Santa Ana, M.; Mendizábal, F.; González, G. *Coord. Chem. Rev.* **2002**, *224*, 87−109.
(41) Hagenbach, G.; Courty, P.; Delmon, B. *J. Catal.* **1971**, *23*, 295−298.
(42) Anderson, A. B.; Al-Saigh, Z. Y.; Hall, W. K. *J. Phys. Chem.* **1988**, *92*, 803−809.
(43) Byskov, L. S.; Bollinger, M.; Nørskov, J. K.; Clausen, B. S.; Topsøe, H. *J. Mol. Catal. A: Chem.* **2000**, *163*, 117−122.
(44) Hemschemeier, A.; Fouchard, S.; Cournac, L.; Peltier, G.; Happe, T. *Planta* **2008**, *227*, 397−407.
(45) Das, D.; Veziroğlu, T. N. *Int. J. Hydrogen Energy* **2001**, *26*, 13−28.
(46) Hallenbeck, P. C.; Benemann, J. R. *Int. J. Hydrogen Energy* **2002**, *27*, 1185−1193.
(47) Markovic, N.; Grgur, B.; Ross, P. *J. Phys. Chem. B* **1997**, *101*, 5405−5413.
(48) Markovic, N. M. *Nat. Mater.* **2013**, *12*, 101−102.
(49) Zinola, C. F.; Martins, M. E.; Tejera, E. P.; Neves, N. P. *Int. J. Electrochem.* **2012**, *10*, 874687.
(50) Benck, J. D.; Chen, Z. B.; Kuritzky, L. Y.; Forman, A. J.; Jaramillo, T. F. *ACS Catal.* **2012**, *2*, 1916−1923.
(51) Bian, X. J.; Zhu, J.; Liao, L.; Scanlon, M. D.; Ge, P. Y.; Ji, C.; Girault, H. H.; Liu, B. H. *Electrochem. Commun.* **2012**, *22*, 128−132.
(52) Bonde, J.; Moses, P. G.; Jaramillo, T. F.; Nørskov, J. K.; Chorkendorff, I. *Faraday Discuss.* **2009**, *140*, 219−231.
(53) Chen, T. Y.; Chang, Y. H.; Hsu, C. L.; Wei, K. H.; Chiang, C. Y.; Li, L. J. *Int. J. Hydrogen Energy* **2013**, *38*, 12302−12309.
(54) Chen, Z.; Cummins, D.; Reinecke, B. N.; Clark, E.; Sunkara, M. K.; Jaramillo, T. F. *Nano Lett.* **2011**, *11*, 4168−4175.
(55) Jaramillo, T. F.; Bonde, J.; Zhang, J.; Ooi, B.-L.; Andersson, K.; Ulstrup, J.; Chorkendorff, I. *J. Phys. Chem. C* **2008**, *112*, 17492−17498.
(56) Ji, S. S.; Yang, Z.; Zhang, C.; Liu, Z. Y.; Tjiu, W. W.; Phang, I. Y.; Zhang, Z.; Pan, J. S.; Liu, T. X. *Electrochim. Acta* **2013**, *109*, 269−275.
(57) Karunadasa, H. I.; Montalvo, E.; Sun, Y. J.; Majda, M.; Long, J. R.; Chang, C. J. *Science* **2012**, *335*, 698−702.
(58) Kibsgaard, J.; Chen, Z.; Reinecke, B. N.; Jaramillo, T. F. *Nat. Mater.* **2012**, *11*, 963−969.
(59) Kong, D. S.; Wang, H. T.; Cha, J. J.; Pasta, M.; Koski, K. J.; Yao, J.; Cui, Y. *Nano Lett.* **2013**, *13*, 1341−1347.

(60) Lau, V. W. H.; Masters, A. F.; Bond, A. M.; Maschmeyer, T. *ChemCatChem* **2011**, *3*, 1739−1742.
(61) Lau, V. W. H.; Masters, A. F.; Bond, A. M.; Maschmeyer, T. *Chem.—Eur. J.* **2012**, *18*, 8230−8239.
(62) Laursen, A. B.; Vesborg, P. C. K.; Chorkendorff, I. *Chem. Commun.* **2013**, *49*, 4965−4967.
(63) Li, Y.; Wang, H.; Xie, L.; Liang, Y.; Hong, G.; Dai, H. *J. Am. Chem. Soc.* **2011**, *133*, 7296−7299.
(64) Liao, L.; Zhu, J.; Bian, X. J.; Zhu, L. N.; Scanlon, M. D.; Girault, H. H.; Liu, B. H. *Adv. Funct. Mater.* **2013**, *23*, 5326−5333.
(65) Lin, T. W.; Liu, C. J.; Lin, J. Y. *Appl. Catal., B* **2013**, *134*, 75−82.
(66) Lu, Z. Y.; Zhang, H. C.; Zhu, W.; Yu, X. Y.; Kuang, Y.; Chang, Z.; Lei, X. D.; Sun, X. M. *Chem. Commun.* **2013**, *49*, 7516−7518.
(67) Lukowski, M. A.; Daniel, A. S.; Meng, F.; Forticaux, A.; Li, L.; Jin, S. *J. Am. Chem. Soc.* **2013**, *135*, 10274−10277.
(68) Lv, X. J.; She, G. W.; Zhou, S. X.; Li, Y. M. *RSC Adv.* **2013**, *3*, 21231−21236.
(69) Merki, D.; Fierro, S.; Vrubel, H.; Hu, X. L. *Chem. Sci.* **2011**, *2*, 1262−1267.
(70) Merki, D.; Vrubel, H.; Rovelli, L.; Fierro, S.; Hu, X. *Chem. Sci.* **2012**, *3*, 2515−2525.
(71) Voiry, D.; Salehi, M.; Silva, R.; Fujita, T.; Chen, M.; Asefa, T.; Shenoy, V. B.; Eda, G.; Chhowalla, M. *Nano Lett.* **2013**, *13*, 6222−6227.
(72) Vrubel, H.; Merki, D.; Hu, X. *Energy Environ. Sci.* **2012**, *5*, 6136−6144.
(73) Vrubel, H.; Moehl, T.; Gratzel, M.; Hu, X. L. *Chem. Commun.* **2013**, *49*, 8985−8987.
(74) Wang, D. Z.; Wang, Z. P.; Wang, C. L.; Zhou, P.; Wu, Z. Z.; Liu, Z. H. *Electrochem. Commun.* **2013**, *34*, 219−222.
(75) Wang, H. T.; Lu, Z. Y.; Xu, S. C.; Kong, D. S.; Cha, J. J.; Zheng, G. Y.; Hsu, P. C.; Yan, K.; Bradshaw, D.; Prinz, F. B.; Cui, Y. *Proc. Natl. Acad. Sci. U.S.A.* **2013**, *110*, 19701−19706.
(76) Yu, Y.; Huang, S.-Y.; Li, Y.; Steinmann, S. N.; Yang, W.; Cao, L. *Nano Lett.* **2014**, *14*, 553−558.
(77) Chen, Z.; Forman, A. J.; Jaramillo, T. F. *J. Phys. Chem. C* **2013**, *117*, 9713−9722.
(78) Chen, Z.; Jaramillo, T. F.; Deutsch, T. G.; Kleiman-Shwarsctein, A.; Forman, A. J.; Gaillard, N.; Garland, R.; Takanabe, K.; Heske, C.; Sunkara, M. *J. Mater. Res.* **2010**, *25*, 3.
(79) Pinaud, B. A.; Benck, J. D.; Seitz, L. C.; Forman, A. J.; Chen, Z.; Deutsch, T. G.; James, B. D.; Baum, K. N.; Baum, G. N.; Ardo, S. *Energy Environ. Sci.* **2013**, *6*, 1983−2002.
(80) Seitz, L. C.; Chen, Z.; Forman, A. J.; Pinaud, B. A.; Benck, J. D.; Jaramillo, T. F. *ChemSusChem* **2014**, *7*, 1372−1385.
(81) Wang, H.; Lu, Z.; Kong, D.; Sun, J.; Hymel, T. M.; Cui, Y. *ACS Nano* **2014**, *8*, 4940−4947.
(82) Savadogo, O.; Lee, K.; Oishi, K.; Mitsushima, S.; Kamiya, N.; Ota, K.-I. *Electrochem. Commun.* **2004**, *6*, 105−109.
(83) Gasteiger, H. A.; Kocha, S. S.; Sompalli, B.; Wagner, F. T. *Appl. Catal., B* **2005**, *56*, 9−35.
(84) Trasatti, S.; Petrii, O. A. *J. Electroanal. Chem.* **1992**, *327*, 353−376.
(85) Brunauer, S.; Emmett, P. H.; Teller, E. *J. Am. Chem. Soc.* **1938**, *60*, 309−319.
(86) Shao, M.; Odell, J. H.; Choi, S.-I.; Xia, Y. *Electrochem. Commun.* **2013**, *31*, 46−48.
(87) Hachiya, T.; Honbo, H.; Itaya, K. *J. Electroanal. Chem. Interfacial Electrochem.* **1991**, *315*, 275−291.
(88) Herrero, E.; Buller, L. J.; Abruna, H. D. *Chem. Rev.* **2001**, *101*, 1897−1930.
(89) Engelsmann, K.; Lorenz, W.; Schmidt, E. *J. Electroanal. Chem. Interfacial Electrochem.* **1980**, *114*, 1−10.
(90) Gasteiger, H. A.; Markovic, N. M.; Ross, P. N., Jr *J. Phys. Chem.* **1995**, *99*, 8290−8301.
(91) Bockris, J. O. M.; Potter, E. C. *J. Electrochem. Soc.* **1952**, *99*, 169−186.
(92) Conway, B. E.; Bockris, J. O.; Apos, M. *J. Chem. Phys.* **1957**, *26*, 532−541.
(93) Kuhl, K. P.; Cave, E. R.; Abram, D. N.; Jaramillo, T. F. *Energy Environ. Sci.* **2012**, *5*, 7050−7059.
(94) Wang, T.; Liu, L.; Zhu, Z.; Papakonstantinou, P.; Hu, J.; Liu, H.; Li, M. *Energy Environ. Sci.* **2013**, *6*, 625−633.
(95) Tokash, J. C.; Logan, B. E. *Int. J. Hydrogen Energy* **2011**, *36*, 9439−9445.
(96) Kibsgaard, J.; Jaramillo, T. F.; Besenbacher, F. *Nat. Chem.* **2014**, *6*, 248−253.
(97) Wu, Z.; Fang, B.; Wang, Z.; Wang, C.; Liu, Z.; Liu, F.; Wang, W.; Alfantazi, A.; Wang, D.; Wilkinson, D. P. *ACS Catal.* **2013**, *3*, 2101−2107.
(98) Jacobson, A. J.; Chianelli, R. R.; Rich, S. M.; Whittingham, M. S. *Mater. Res. Bull.* **1979**, *14*, 1437−1448.
(99) Liang, K. S.; Cramer, S. P.; Johnston, D. C.; Chang, C. H.; Jacobson, A. J.; Deneufville, J. P.; Chianelli, R. R. *J. Non-Cryst. Solids* **1980**, *42*, 345−356.
(100) Chang, C. H.; Chan, S. S. *J. Catal.* **1981**, *72*, 139−148.
(101) Bhattacharya, R. N.; Lee, C. Y.; Pollak, F. H.; Schleich, D. M. *J. Non-Cryst. Solids* **1987**, *91*, 235−242.
(102) Belanger, D.; Laperriere, G.; Marsan, B. *J. Electroanal. Chem.* **1993**, *347*, 165−183.
(103) Weber, T.; Muijsers, J. C.; Niemantsverdriet, J. W. *J. Phys. Chem.* **1995**, *99*, 9194−9200.
(104) Hibble, S. J.; Walton, R. I.; Pickup, D. M.; Hamon, A. C. *J. Non-Cryst. Solids* **1998**, *232*, 434−439.
(105) Ge, X.; Chen, L.; Zhang, L.; Wen, Y.; Hirata, A.; Chen, M. *Adv. Mater.* **2014**, *26*, 3100−3104.
(106) Laursen, A. B.; Pedersen, T.; Malacrida, P.; Seger, B.; Hansen, O.; Vesborg, P. C. K.; Chorkendorff, I. *Phys. Chem. Chem. Phys.* **2013**, *15*, 20000−20004.
(107) Seger, B.; Laursen, A. B.; Vesborg, P. C. K.; Pedersen, T.; Hansen, O.; Dahl, S.; Chorkendorff, I. *Angew. Chem., Int. Ed.* **2012**, *51*, 9128−9131.
(108) Tang, M. L.; Grauer, D. C.; Lassalle-Kaiser, B.; Yachandra, V. K.; Amirav, L.; Long, J. R.; Yano, J.; Alivisatos, A. P. *Angew. Chem.* **2011**, *123*, 10385−10389.
(109) Hou, Y. D.; Abrams, B. L.; Vesborg, P. C. K.; Bjorketun, M. E.; Herbst, K.; Bech, L.; Setti, A. M.; Damsgaard, C. D.; Pedersen, T.; Hansen, O.; Rossmeisl, J.; Dahl, S.; Norskov, J. K.; Chorkendorff, I. *Nat. Mater.* **2011**, *10*, 434−438.
(110) Müller, A.; Krickemeyer, E.; Hadjikyriacou, A.; Coucouvanis, D. In *Inorganic Syntheses*; Ginsberg, A. P., Ed.; John Wiley & Sons, Inc.: New York, 2007; Vol. *27*, pp 47−51.
(111) Benjamin, T. G.; Epping-Martin, K.; Garland, N. L.; Ho, D. L.; Kopasz, J. P.; Papageorgopoulos, D. C.; Podolski, W. F. *ECS Trans.* **2013**, *50*, 1315−1320.
(112) Tauster, S.; Pecoraro, T.; Chianelli, R. *J. Catal.* **1980**, *63*, 515−519.
(113) Chianelli, R. *Catal. Rev.: Sci. Eng.* **1984**, *26*, 361−393.
(114) Okamoto, Y.; Maezawa, A.; Imanaka, T. *J. Catal.* **1989**, *120*, 29−45.
(115) Bouwens, S.; Van Veen, J.; Koningsberger, D.; De Beer, V.; Prins, R. *J. Phys, Chem.* **1991**, *95*, 123−134.
(116) Lauritsen, J.; Kibsgaard, J.; Olesen, G.; Moses, P.; Hinnemann, B.; Helveg, S.; Norskov, J.; Clausen, B.; Topsoe, H.; Lagsgaard, E. *J. Catal.* **2007**, *249*, 220−233.
(117) Byskov, L. S.; Hammer, B.; Nørskov, J. K.; Clausen, B. S.; Topsøe, H. *Catal. Lett.* **1997**, *47*, 177−182.
(118) Besenbacher, F.; Brorson, M.; Clausen, B. S.; Helveg, S.; Hinnemann, B.; Kibsgaard, J.; Lauritsen, J. V.; Moses, P. G.; Nørskov, J. K.; Topsøe, H. *Catal. Today* **2008**, *130*, 86−96.
(119) Lauritsen, J.; Helveg, S.; Lægsgaard, E.; Stensgaard, I.; Clausen, B. S.; Topsoe, H.; Besenbacher, F. *J. Catal.* **2001**, *197*, 1−5.
(120) Kibsgaard, J.; Tuxen, A.; Knudsen, K. G.; Brorson, M.; Topsøe, H.; Lægsgaard, E.; Lauritsen, J. V.; Besenbacher, F. *J. Catal.* **2010**, *272*, 195−203.
(121) Wang, H. T.; Kong, D. S.; Johanes, P.; Cha, J. J.; Zheng, G. Y.; Yan, K.; Liu, N. A.; Cui, Y. *Nano Lett.* **2013**, *13*, 3426−3433.

(122) Sun, X.; Dai, J.; Guo, Y.; Wu, C.; Hu, F.; Zhao, J.; Zeng, X. C.; Xie, Y. *Nanoscale* **2014**, *6*, 8359−8367.
(123) Tsai, C.; Abild-Pedersen, F.; Nørskov, J. K. *Nano Lett.* **2014**, *14*, 1381−1387.
(124) Chen, W.; Santos, E. J. G.; Zhu, W. G.; Kaxiras, E.; Zhang, Z. Y. *Nano Lett.* **2013**, *13*, 509−514.
(125) Sheng, W.; Gasteiger, H. A.; Shao-Horn, Y. *J. Electrochem. Soc.* **2010**, *157*, B1529−B1536.
(126) Li, D. J.; Maiti, U. N.; Lim, J.; Choi, D. S.; Lee, W. J.; Oh, Y.; Lee, G. Y.; Kim, S. O. *Nano Lett.* **2014**, *14*, 1228−1233.
(127) Fujishima, A.; Noguchi, Y.; Honda, K.; Loo, B. H. *Bull. Chem. Soc. Jpn.* **1982**, *55*, 17−22.
(128) Gobrecht, J.; Tributsch, H.; Gerischer, H. *J. Electrochem. Soc.* **1978**, *125*, 2085−2086.
(129) Kautek, W.; Gerischer, H. *Ber. Bunsen-Ges.* **1980**, *84*, 645−653.
(130) Kiesewetter, T.; Tomm, Y.; Turrion, M.; Tributsch, H. *Sol. Energy Mater. Sol. Cells* **1999**, *59*, 309−323.
(131) Kubiak, C. P.; Schneemeyer, L. F.; Wrighton, M. S. *J. Am. Chem. Soc.* **1980**, *102*, 6898−6900.
(132) Schneemeyer, L. F.; Wrighton, M. S. *J. Am. Chem. Soc.* **1979**, *101*, 6496−6500.
(133) Wilcoxon, J. P.; Samara, G. A. *Phys. Rev. B, Condens. Matter* **1995**, *51*, 7299−7302.
(134) Frame, F. A.; Osterloh, F. E. *J. Phys. Chem. C* **2010**, *114*, 10628−10633.
(135) Huang, Z. P.; Wang, C. F.; Pan, L.; Tian, F.; Zhang, X. X.; Zhang, C. *Nano Energy* **2013**, *2*, 1337−1346.
(136) King, H. W. In *CRC handbook of chemistry and physics: a ready-reference book of chemical and physical data*, 94th ed.; Haynes, W. M., Ed.; CRC Press: Boca Raton, FL, 2013.
(137) Liu, Y.; Yu, Y. X.; Zhang, W. D. *J. Phys. Chem. C* **2013**, *117*, 12949−12957.
(138) Maitra, U.; Gupta, U.; De, M.; Datta, R.; Govindaraj, A.; Rao, C. N. R. *Angew. Chem., Int. Ed.* **2013**, *52*, 13057−13061.
(139) Wei, L.; Chen, Y. J.; Lin, Y. P.; Wu, H. S.; Yuan, R. S.; Li, Z. H. *Appl. Catal., B* **2014**, *144*, 521−527.
(140) Xiang, Q. J.; Yu, J. G.; Jaroniec, M. *J. Am. Chem. Soc.* **2012**, *134*, 6575−6578.
(141) Zong, X.; Wu, G. P.; Yan, H. J.; Ma, G. J.; Shi, J. Y.; Wen, F. Y.; Wang, L.; Li, C. *J. Phys. Chem. C* **2010**, *114*, 1963−1968.
(142) Zong, X.; Yan, H.; Wu, G.; Ma, G.; Wen, F.; Wang, L.; Li, C. *J. Am. Chem. Soc.* **2008**, *130*, 7176−7177.
(143) Xiang, Q.; Yu, J.; Jaroniec, M. *J. Am. Chem. Soc.* **2012**, *134*, 6575−6578.
(144) Tran, P. D.; Pramana, S. S.; Kale, V. S.; Nguyen, M.; Chiam, S. Y.; Batabyal, S. K.; Wong, L. H.; Barber, J.; Loo, J. *Chem.−Eur. J.* **2012**, *18*, 13994−13999.
(145) Gao, L.; Cui, Y.; Wang, J.; Cavalli, A.; Standing, A.; Vu, T.; Verheijen, M.; Haverkort, J.; Bakkers, E. P.; Notten, P. H. *Nano Lett.* **2014**, *14*, 3715−3719.
(146) Ding, Q.; Meng, F.; English, C. R.; Cabán-Acevedo, M.; Shearer, M. J.; Liang, D.; Daniel, A. S.; Hamers, R. J.; Jin, S. *J. Am. Chem. Soc.* **2014**, *136*, 8504−8507.
(147) Zhao, Y.-F.; Yang, Z.-Y.; Zhang, Y.-X.; Jing, L.; Guo, X.; Ke, Z.; Hu, P.; Wang, G.; Yan, Y.-M.; Sun, K.-N. *J. Phys. Chem. C* **2014**, *26*, 14238−14245.
(148) Chang, K.; Mei, Z.; Wang, T.; Kang, Q.; Ouyang, S.; Ye, J. *ACS Nano* **2014**, *8*, 7078−7087.
(149) Benck, J. D.; Lee, S. C.; Fong, K. D.; Kibsgaard, J.; Sinclair, R.; Jaramillo, T. F. *Adv. Energy Mater.* **2014**, 10.1002/aenm.201400739.
(150) Ayers, K. E.; Anderson, E. B.; Capuano, C.; Carter, B.; Dalton, L.; Hanlon, G.; Manco, J.; Niedzwiecki, M. *ECS Trans.* **2010**, *33*, 3−15.
(151) Ivy, J. *Summary of electrolytic hydrogen production: milestone completion report*; National Renewable Energy Lab.: Golden, CO, 2004.
(152) Goni-Urtiaga, A.; Presvytes, D.; Scott, K. *Int. J. Hydrogen Energy* **2012**, *37*, 3358−3372.
(153) Vesborg, P. C. K.; Jaramillo, T. F. *RSC Adv.* **2012**, *2*, 7933−7947.
(154) Laursen, A. B.; Vesborg, P. C. K.; Chorkendorff, I. *Chem. Commun.* **2013**, *49*, 4965−4967.